Preparation by High-Energy Milling, Characterization, and Catalytic Properties of Nanocrystalline TiO_2

Sylvio Indris,*,† Roger Amade,† Paul Heitjans,† Mina Finger,‡ Andreas Haeger,‡ Diethard Hesse,‡ Wolfgang Grünert,§ Alexander Börger,|| and Klaus Dieter Becker||

Institut für Physikalische Chemie und Elektrochemie, Universität Hannover, Callinstrasse 3-3A, 30167 Hannover, Germany, Institut für Technische Chemie, Universität Hannover, Callinstrasse 3, 30167 Hannover, Germany, Lehrstuhl für Technische Chemie, Ruhr-Universität Bochum, Universitätsstrasse 150, 44780 Bochum, Germany, and Institut für Physikalische und Theoretische Chemie, Technische Universität Braunschweig, Hans-Sommer-Strasse 10, 38106 Braunschweig, Germany

Received: August 15, 2005; In Final Form: October 11, 2005

Titanium dioxide (TiO_2) is widely used for applications in heterogeneous photocatalysis. We prepared nanocrystalline powders of the anatase as well as the rutile modification by high-energy ball milling of the coarse grained source materials for up to 4 h. The resulting average grain size was about 20 nm. The morphology of the powders was investigated with transmission electron microscopy, X-ray powder diffraction, and BET surface area determination. Measurements of the catalytic activity reveal a maximum as a function of the milling time at about 40 min. This maximum could be explained by a superposition of two counteracting effects. The first one is the increase of the specific surface area resulting in an increase of the catalytic activity, and the second one is a change of the electronic structure at the surface of the TiO_2 particles corresponding to a reduction of the surface. The latter one was confirmed by light absorption experiments, X-ray photoelectron spectroscopy, and electron paramagnetic resonance spectroscopy.

1. Introduction

Titanium dioxide is a photosemiconducting material with a band-gap of about 3.2 eV that can be used in photoinduced heterogeneous catalysis.[1] Though the material is excessively studied and applied, the relations between structural and catalytic properties are poorly understood.

We investigated the catalytic activity of TiO_2 powders in the anatase and rutile forms with different grain sizes in the range from about 1 μm down to about 20 nm. Anatase and rutile are crystalline structures belonging to space groups $I4_1/amd$ (anatase) and $P4_2/mnm$ (rutile), respectively. Both consist of regular networks of TiO_6 octahedra. Investigations on single crystals of rutile in ultrahigh vacuum revealed that the surface structure is influenced by the bulk reduction state of TiO_2 and that there is a strong correlation between bulk structure and the surface properties.[2,3]

High-energy milling leads to a reduction in grain size and a corresponding increase of the surface area as well as to a modification of the surface structure. The effect of the increased surface area and interfacial regions on ion transport in nanocrystalline materials has been the subject of previous studies (refs 4 and 5 and references therein). The aim of the present work is to investigate the influence of mechanical attrition on structure and photocatalytic activity of TiO_2. To get an in-depth characterization of the powder samples we studied their structure by means of transmission electron microscopy (TEM), X-ray powder diffraction (XRD), and BET surface area determination (BET). Additionally, the electronic structure of the samples was investigated using diffuse reflectance spectroscopy, X-ray photoelectron spectroscopy (XPS), and electron paramagnetic resonance spectroscopy (EPR).

2. Experimental Section

To investigate the reaction rate of the gas reactions, the catalyst material was fixed as a thin layer on a stainless steel plate (57 cm^2). In the reactor, this catalytically active plate together with a glass plate (DURAN, Schott) form the reaction chamber (see Figure 1). The plate is irradiated through a filter absorbing IR light of the medium-pressure UV lamp (Philips HPA 1000/20). To adjust the irradiation intensity, the distance between the plate and the lamp can be varied. The spectrum $I_0(\lambda)$ of the radiation at the catalyst surface was measured with a diode-array spectrometer. To calculate the absorbed irradiation intensity I_p, the absorption coefficient $\alpha(\lambda)$ of the active plate was measured as a function of the wavelength λ by means of diffuse reflectance spectroscopy using an integrating sphere of Teflon (DMC25, CarlZeissGmbH).

The photoreactor was mounted into the experimental setup as shown schematically in Figure 1. It consists of the gas supply system, the reaction system and the analytic system. The flow rates of the gases were adjusted by flow meters, and the gases were mixed in a mixing chamber. The reactor operates as a continuous stirred tank reactor in order to avoid local concentration gradients along the flow direction in the reaction chamber. This operation mode was achieved by recycling the effluent gas very quickly compared to the incoming gas flow rate. The composition of the incoming as well as that of the effluent gas was determined by means of an FTIR analyzer (BrukerIFS28). The temperature of the catalyst plate was adjusted by means of a heating plate and controlled by a thermocouple. Using the steady-state material balance equation, the reaction rate r_A per

* Corresponding author. Tel.: +49−511-762-5453, Fax.: +49−511-762-19121, e-mail: indris@pci.uni-hannover.de

† Institut für Physikalische Chemie und Elektrochemie, Universität Hannover.

‡ Institut für Technische Chemie, Universität Hannover.

§ Ruhr-Universität Bochum.

|| Technische Universität Braunschweig.

10.1021/jp054586t CCC: $30.25
Published on Web 11/17/2005

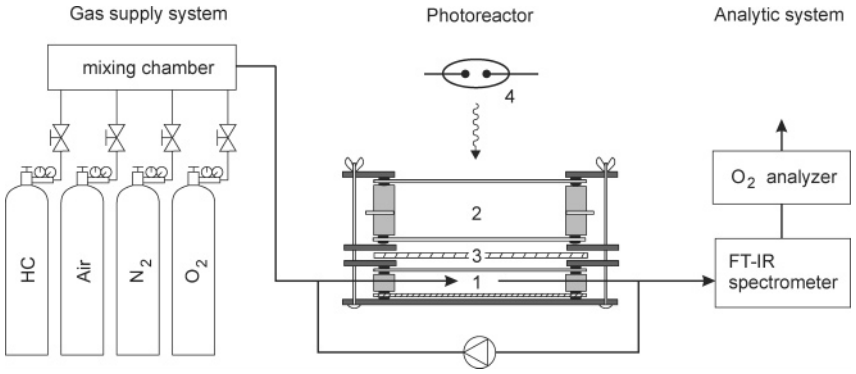

Figure 1. Sketch of the experimental setup for the catalytic measurements: (1) reaction chamber with catalyst; (2) infrared filter; (3) band-pass filter; (4) Hg medium-pressure arc lamp.

surface area A of a given reaction was calculated for a given flow rate $\dot{V}$ with the help of the concentration of a reaction component i in the incoming (c_i^0) and the effluent (c_i) flow according to

$$r_A = \frac{\dot{V}}{A}(c_i^0 - c_i) \tag{1}$$

The quantum yield Q [%] characterizes the reaction system. It is defined by

$$Q = \frac{r_A}{I_p^*}100 \tag{2}$$

where I_p^* denotes the moles of photons absorbed per second and geometric surface area of the photocatalytically active plate (for details see ref 6).

XRD measurements were performed with a Philips X'Pert MPD system using Cu K_α radiation. The TEM pictures were taken on a TecnaiF20 STEM (FEI company) equipped with an S-TWIN objective lens and a field emission gun. The BET surface area was determined with a Gemini 2375 surface analyzer (Micromeritics). XPS spectra were measured with a LeyboldLH 10 spectrometer equipped with an EA 10/100 multichannel detector (Specs), using Mg Kα excitation (1253.6 eV, 10 kV $\times$ 20 mA). The binding-energy scale was referenced to the binding energy of adventitious carbon (C 1s = 284.5 eV). Samples were analyzed after contact with air. EPR spectra were recorded at 100 K with a Bruker EMX X-band spectrometer between 100 G and 6900 G using a modulation amplitude of 10 G, a modulation frequency of 100 kHz, and a time constant of 20.48 ms.

3. Sample Preparation

The nanocrystalline powders were prepared from the unmilled samples (Acros, 99.5%) by high-energy ball milling. We used a SPEX8000 ball mill with an alumina vial and a single alumina ball. The ball-to-powder weight ratio was 2:1. The standard preparation method was dry milling in air for up to 4 h. Furthermore, we tested the influence of milling in liquid nitrogen to check whether low temperatures lead to even smaller grain sizes due to an enhanced brittleness. Since the nitrogen evaporates very rapidly during milling, the vial had to be filled every five minutes. For the samples milled for 4 h, comparative studies were done after annealing in NO_2 to check the influence of reduction of the sample surfaces, which was assumed to occur during milling.

4. Sample Characterization

High-energy ball milling of ceramic powders can reduce the average crystallite sizes from the μm regime down to some nm.[7]

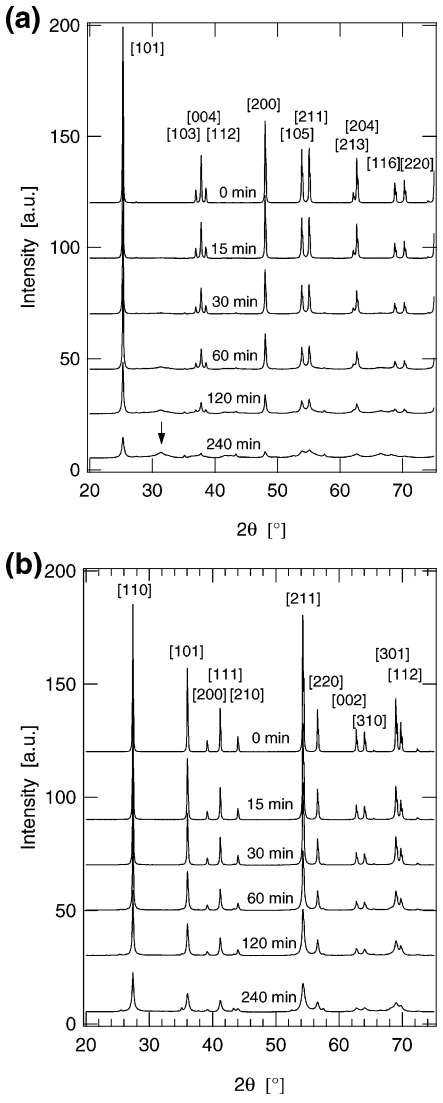

Figure 2. XRD powder patterns of (a) anatase and (b) rutile milled for up to 4 h. XRD was done using Cu K_α radiation. The arrow in (a) marks the formation of a high-pressure phase.

Variation of the milling time allows for a well-defined adjustment of the average grain size. A standard method to determine the average grain sizes in powder samples is the evaluation of the line broadening in XRD patterns. Figure 2 shows the XRD pattern for anatase and rutile powders, respectively, milled for up to 4 h in comparison with the unmilled samples. They exhibit an increasing broadening of the XRD peaks with increasing milling time. Evaluation via the Scherrer equation[8]

$$L_0 = \frac{K\lambda}{\beta\cos\theta} \tag{3}$$

(K = Scherrer constant, λ = X-ray wavelength, β = width of the XRD peak after corrections concerning instrumental broadening, θ = diffraction angle) gives the average crystallite size L_0 vs milling time (Figure 3). The results for anatase and rutile show that the average grain size could be varied between some μm (unmilled samples) and about 20 nm. For a detailed study of possible pitfalls in the determination of grain sizes of anatase powders by XRD, TEM, and BET surface area, see ref 9.

An additional feature shows up for the anatase powder. A broad peak arises during milling at a diffraction angle of about 31.4°, see Figure 2a. It can be attributed to a high-pressure phase of TiO_2 (α-PbO_2-type structure[10]). Since this peak is much broader than the original anatase peaks, it may be concluded that the new phase is formed on the surface of the anatase particles resulting in a thin cover layer.[11,12]

To get a verification for the crystallite sizes, TEM was performed on rutile powders milled for 4 h. Figure 4 shows an example for a micrograph with atomic resolution. The line patterns reveal the crystallographic orientation of the crystallites and in fact show sizes of about 20 nm, which is in good agreement with the XRD results.

The reduction in the average crystallite size should be accompanied by an increase in the specific surface area of the powders. The BET surface area vs milling time is shown in Figure 5 for anatase and rutile samples. The surface area increases monotonically with increasing milling time for both samples. Nevertheless the increase (by a factor of about three in the case of rutile) is much smaller than the decrease of the crystallite size (by about 3 orders of magnitude). This has to be attributed to the formation of compacted agglomerates during milling.

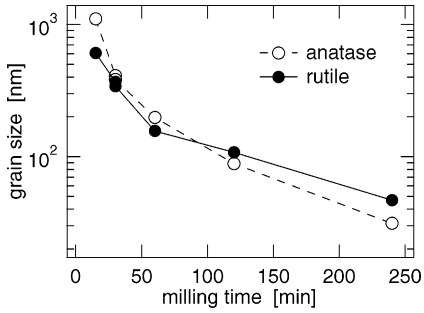

Figure 3. Average particle size versus milling time for rutile and anatase.

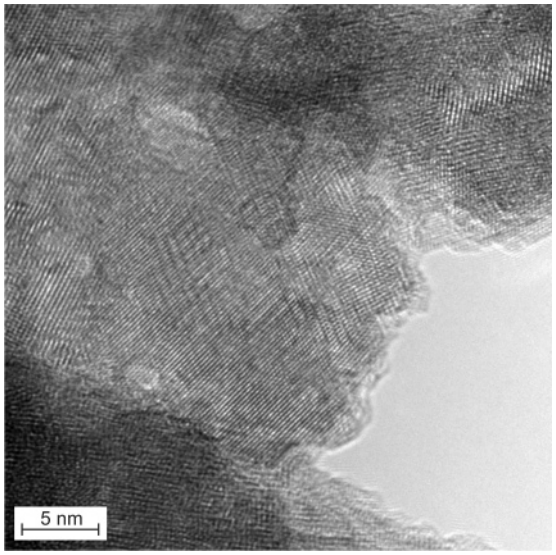

Figure 4. TEM micrograph of rutile ball-milled for 4 h.

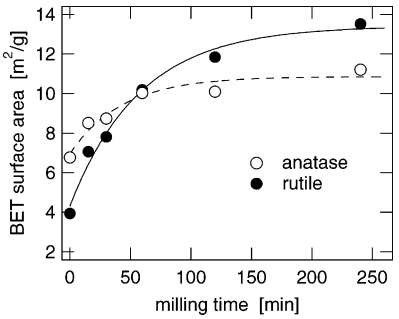

Figure 5. BET surface area versus milling time for rutile and anatase.

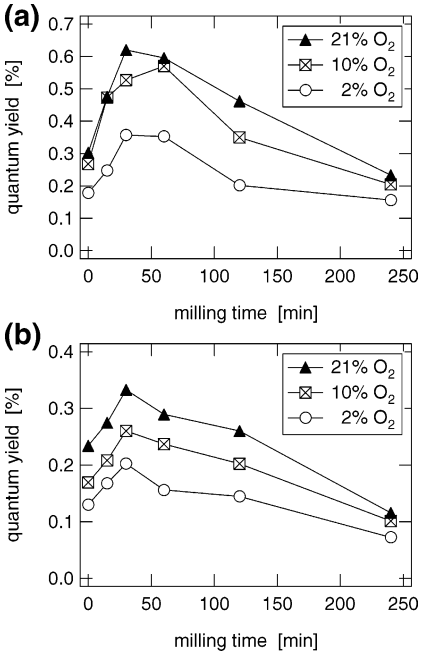

Figure 6. Quantum yield for the combustion of hydrocarbons (eq 4) at 433 K on (a) anatase and (b) rutile powders for milling times of up to 4 h and different concentrations of oxygen. N_2 was used as carrier gas. The concentration of propane was 300 ppm.

5. Results

5.1. Catalytic Activity. To study the catalytic activity of the TiO_2 powders, the combustion of propane was taken as an example:

$$C_3H_8 + 5O_2 \xrightarrow{h\nu,\ TiO_2} 3CO_2 + 4H_2O \tag{4}$$

Figure 6 shows the results for the quantum yield Q, defined by eq 2, as a function of milling time for anatase and rutile powders for given concentrations of oxygen and a fixed value of propane concentration (300 ppm). The temperature was T = 433 K in all experiments. All curves show a distinct maximum for a milling time of about 45 min. For the anatase powder, the initial increase in the quantum yield is even stronger than the increase in the BET surface area (cf. Figure 5), which suggests a qualitative modification of the surface. For milling times longer than about 50 min the quantum yield is decreasing for both materials, which reveals some kind of degradation of the TiO_2 surface.

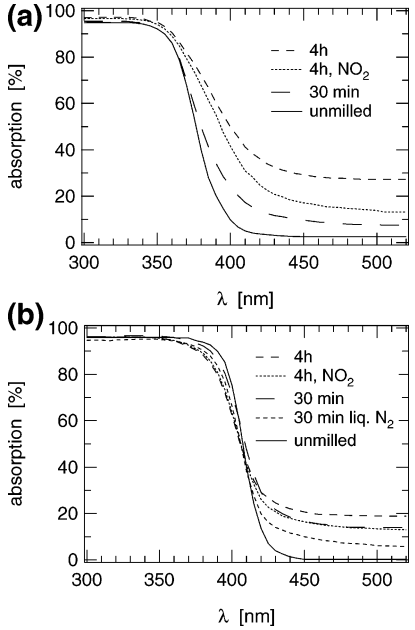

Figure 7. Light absorption by (a) anatase and (b) rutile, respectively, milled for up to 4 h, determined by diffuse reflectance spectroscopy.

5.2. Electronic Structure. The decrease of the quantum yield for long milling times hints at a modification of the electronic structure at the surface of the TiO_2 particles. This was investigated by diffuse reflectance measurements on anatase (Figure 7a) and rutile (Figure 7b). The figures show that with increasing milling time an increasing absorption for wavelengths larger than 400 nm occurs for both modifications. This reveals the formation of additional electronic states in the band gap at the surface of the TiO_2 particles, in anatase as well as in rutile. The measurements on the samples milled for 4 h were repeated after an annealing treatment in NO_2 atmosphere at 433 K for 1 day. By this, the absorption in the band gap could be reduced which shows that the modification in the electronic structure is caused by a partial, reversible reduction of the TiO_2 surface. For the rutile powder, milling was also done in liquid nitrogen for 30 min. Comparison with the result for the sample milled in air shows that the absorption in the band gap is lower and hence the distortion of the electronic structure is weaker when milling is performed in liquid nitrogen.

The electronic structure in the surface of the TiO_2 powders was also investigated by means of XPS. Figure 8 shows results on the Ti 2p doublet for unmilled anatase and anatase milled for 4 h. Comparison of both curves shows that the spectrum of the milled sample exhibits a slight but significant asymmetry toward lower binding energies (inset). The new signal that is required to reproduce the signal shape (dashed line) has a binding energy of 0.9 eV below that of Ti^{4+} (457.8 eV) and may be assigned to Ti^{3+}. This confirms the partial reduction of the samples during milling. XPS results for the rutile modification, not shown here, are very similar.

To verify the formation of Ti^{3+} during milling, we performed EPR measurements on rutile powders milled for up to 4 h. In Figure 9 the EPR spectra are shown with the intensity normalized to the net weight of the different samples. There are two important features in the spectra. These are a narrow signal centered at a *g*-factor value of $g = 1.96$, whose intensity increases monotonically with increasing milling time, and a broad, asymmetric signal centered at $g = 2.42$ that starts to appear after about 2 h of milling. The first signal can be clearly attributed to Ti^{3+}.[13−15] This fully confirms the XPS results and

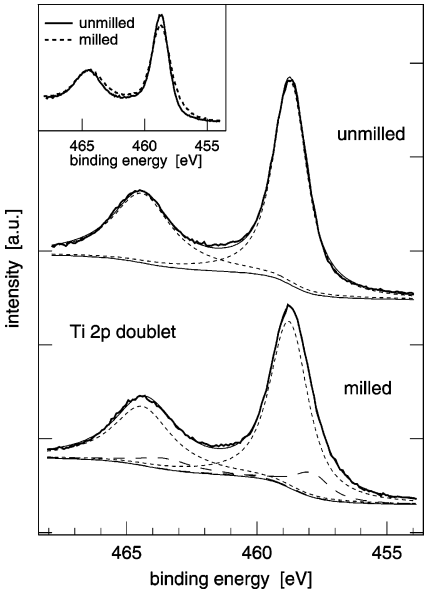

Figure 8. XPS spectra of unmilled anatase and of anatase milled for 4 h. The dotted and dashed lines show the different contributions used to reproduce the experimental data. The inset shows a direct comparison of both spectra.

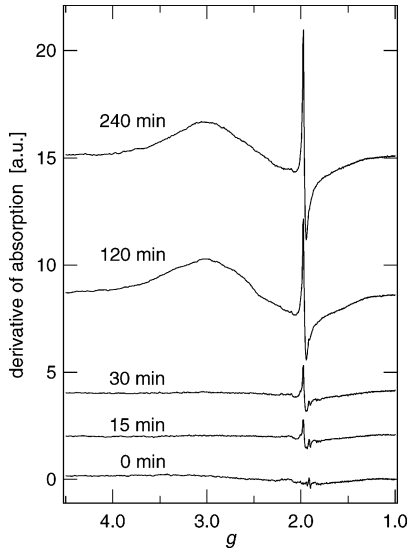

Figure 9. EPR spectra of ball-milled TiO_2 (rutile) at 100 K. The signal intensities are normalized to the sample weight.

shows that the milling leads to a monotonic increase of the Ti^{3+} concentration. The origin of the broad signal is less clear; it might be due to some intermediate oxygen species on the surface which are formed during the excorporation of oxygen.[16]

6. Discussion

The catalytic properties of nanocrystalline TiO_2 powders were found to be strongly influenced by mechanical attrition. The most challenging result is the maximum of the quantum yield as a function of milling time at about 45 min (Figure 6). The maximum cannot be attributed to the change of the BET surface area with milling time, since that is increasing monotonically (Figure 5). Since all the external parameters are constant during the experiments, the maximum has to be caused by a change in material properties. It could be shown by diffuse reflectometry, XPS measurements, and EPR spectroscopy that this change corresponds to a modified electronic structure of the semiconductor. In the case of anatase, even the formation of a high-

pressure phase could be observed by XRD. The formation of this phase during ball milling of TiO_2 anatase was also detected recently by Raman spectroscopy.[17] The exact position of the maximum may be dependent on the ball-to-powder weight ratio since the use of less powder results in a more effective milling process.[12,18]

The EPR measurements show that the Ti^{3+} concentration increases monotonically with increasing milling time. Already after 15 min of milling a clearly detectable amount of Ti^{3+} is present (Figure 9). This, together with the increasing BET surface area, initially increases the reaction rate. The fact that the quantum yield increases even more strongly than the surface area shows that the surface is qualitatively enhanced, i.e., mechanically activated, during the milling process, and that the formation of Ti^{3+} is favorable for increasing the reaction rate at low Ti^{3+} concentrations. The decrease of the quantum yield for long milling times shows that relatively high concentrations of Ti^{3+} ions and thus oxygen defects lead to a dramatic decrease of the quantum yield with increasing defect concentration. Since we know from additional experiments that it is much easier to exchange lattice oxygen reversibly in the lower defect concentration range than in the higher concentration region,[19] we come to the conclusion that oxygen mobility in the surface or in the near surface region is very important for the catalytic properties.

Our results for TiO_2 are consistent with results obtained for other oxide materials. A partial reduction during high-energy ball milling was also observed, e.g., for magnesium ferrite by means of Mössbauer spectroscopy.[20] The relationship between catalytic activity and structural properties was also studied for Bi promoted vanadyl phosphate.[21] In the latter case it has been shown that milling can replace the high-temperature activation of the catalyst.

7. Conclusion

We were able to prepare nanocrystalline TiO_2 powders, both anatase and rutile, by high-energy ball milling. The average grain size could be varied via the milling time in the range from some micrometers down to about 20 nm. We showed that the catalytic activity of TiO_2 powders is strongly influenced by the powder morphology and the electronic structure of the samples. Preparing very fine grained samples by ball milling opens the possibility to a systematic study of the relationship between structural and catalytic properties. For all milling times the decrease of the grain sizes leads to an increase in the BET surface area. For long times, the milling results in a drastic modification of the electronic structure at the surface of the samples, which leads to a decrease of the quantum yield. Subsequent annealing in NO_2 or performing the milling in liquid N_2 are two ways to reduce and prevent, respectively, this structural distortion and thus the decrease in the quantum yield.

Acknowledgment. We are grateful to the Deutsche Forschungsgemeinschaft for financial support. We thank Dr. Christian Kübel (FEI Company, Eindhoven) for the TEM micrographs.

References and Notes

(1) Linsebigler, A. L.; Lu, G.; Yates, J. T., Jr. *Chem. Rev.* **1995**, *95*, 735−758.
(2) Li, M.; Hebenstreit, W.; Diebold, U. *Phys. Rev. B* **2000**, *61*, 4926−4933.
(3) Li, M.; Hebenstreit, W.; Diebold, U.; Tyryshkin, A. M.; Bowman, M. K.; Dunham, G. G.; Henderson, M. A. *J. Phys. Chem. B* **2000**, *104*, 4944−4950.
(4) Heitjans, P.; Indris, S. *J. Mater. Sci.* **2004**, *39*, 5091−5096.
(5) Heitjans, P.; Indris, S. *J. Phys.: Condens. Matter* **2003**, *15*, R1257−R1289.
(6) Haeger, A.; Kleinschmidt, O.; Hesse, D. *Chem. Eng. Technol.* **2004**, *27*, 1019−1026.
(7) Indris, S.; Bork, D.; Heitjans, P. *J. Mater. Synth. Process*. **2000**, *8*, 245−250.
(8) Klug, H. P.; Alexander, L. E. *X-Ray Diffraction Procedures*; John Wiley & Sons: New York, 1959.
(9) Weibel, A.; Bouchet, R.; Boulc'h, F.; Knauth, P. *Chem. Mater.* **2005**, *17*, 2378−2385.
(10) Bendeliani, N. A.; Popova, S. V.; Vereshchagin, L. F. *Geochim. Int.* **1966**, *3*, 387−390.
(11) Begin-Colin, S.; Girot, T.; Mocellin, A.; Le Caër, G. *Nanostruct. Mater.* **1999**, *12*, 195−198.
(12) Girot, T.; Begin-Colin, S.; Devaux, X.; Le Caër, G.; Mocellin, A. *J. Mater. Synth. Proc.* **2000**, *8*, 139−144.
(13) Meriaudeau, P.; Che, M.; Gravelle, P. C.; Teichner, S. J. *Bull. Soc. Chim. Fr.* **1971**, 13−22.
(14) Dyrek, C.; Schindler, R. N. *Z. Naturforsch. N. F.* **1977**, *32A*, 501−504.
(15) Serwicka, E. M. *Z. Phys. Chem.* **1990**, *166*, 249−252.
(16) Merkle, R.; Maier, J. *Phys. Chem. Chem. Phys* **2002**, *4*, 4140−4148.
(17) Gajović, A.; Stubičar, M.; Ivanda, M.; Furić, K. *J. Mol. Struct.* **2001**, *563*−*564*, 315−320.
(18) Takacs, L.; Šepelák, V. *J. Mater. Sci.* **2004**, *39*, 5487−5489.
(19) Amade, R.; Heitjans, P.; Indris, S.; Finger, M.; Haeger, A.; Hesse, D., submitted.
(20) Šepelák, V.; Menzel, M.; Becker, K. D.; Krumeich, F. *J. Phys. Chem. B* **2002**, *106*, 6672−6678.
(21) Ayub, I.; Su, D.; Willinger, M.; Kharlamov, A.; Ushkalov, L.; Zazhigalov, V. A.; Kirillova, N.; Schlögl, R. *Phys. Chem. Chem. Phys.* **2003**, *5*, 970−978.